First identification and modelling of SPI background lines

G. Weidenspointner, J. Kiener, M. Gros, P. Jean, Bj. Teegarden, C. Wunderer, R.C. Reedy, D. Attie, R. Diehl, C. Ferguson, et al.

▶ **To cite this version:**

G. Weidenspointner, J. Kiener, M. Gros, P. Jean, Bj. Teegarden, et al.. First identification and modelling of SPI background lines. Astronomy and Astrophysics - A&A, 2003, 411, pp.L113-L116. 10.1051/0004-6361:20031209 . in2p3-00022236

HAL Id: in2p3-00022236
https://hal.in2p3.fr/in2p3-00022236

Submitted on 15 Jan 2007

HAL is a multi-disciplinary open access archive for the deposit and dissemination of scientific research documents, whether they are published or not. The documents may come from teaching and research institutions in France or abroad, or from public or private research centers.

L'archive ouverte pluridisciplinaire **HAL**, est destinée au dépôt et à la diffusion de documents scientifiques de niveau recherche, publiés ou non, émanant des établissements d'enseignement et de recherche français ou étrangers, des laboratoires publics ou privés.

A&A 411, L113–L116 (2003)
DOI: 10.1051/0004-6361:20031209
© ESO 2003

Astronomy & Astrophysics

First identification and modelling of SPI background lines⋆,⋆⋆

G. Weidenspointner[1,2,3,⋆⋆⋆], J. Kiener[4], M. Gros[5], P. Jean[3], B. J. Teegarden[1], C. Wunderer[6], R. C. Reedy[3,7], D. Attié[5], R. Diehl[6], C. Ferguson[8], M. J. Harris[1,2], J. Knödlseder[3], P. Leleux[9], V. Lonjou[3], J.-P. Roques[3], V. Schönfelder[6], C. Shrader[1,2], S. Sturner[1,2], V. Tatischeff[4], and G. Vedrenne[3]

[1] NASA Goddard Space Flight Center, LHEA, Code 661, Greenbelt, MD 20771, USA
[2] Universities Space Research Association, 7501 Forbes Blvd. #206, Seabrook, MD 20706, USA
[3] Centre d'Étude Spatiale des Rayonnements, 9 avenue Colonel Roche, 31028 Toulouse Cedex 4, France
[4] CSNSM, IN2P3-CNRS and Université Paris-Sud, 91405 Orsay, France
[5] DSM/DAPNIA/SAp, Centre d'Études Nucléaires de Saclay, 91191 Gif-sur-Yvette Cedex, France
[6] Max-Planck-Institut für extraterrestrische Physik, Giessenbachstrasse, 85740 Garching, Germany
[7] University of New Mexico, Albuquerque, NM 87131, USA
[8] Department of Physics and Astronomy, University of Southampton, Southampton SO17 1BJ, UK
[9] Institut de Physique Nucléaire, Université catholique de Louvain, 1348 Louvain-la-Neuve, Belgium

Received 16 July 2003 / Accepted 4 August 2003

Abstract. On Oct. 17, 2002, the ESA INTEGRAL observatory was launched into a highly elliptical orbit. SPI, a high resolution Ge spectrometer covering an energy range of 20–8000 keV, is one of its two main instruments. We use data recorded early in the mission (i.e. in March 2003) to characterize the instrumental background, in particular the many gamma-ray lines produced by cosmic-ray interactions in the instrument and spacecraft materials. More than 300 lines and spectral features are observed, for about 220 of which we provide identifications. An electronic version of this list, which will be updated continuously, is available for download at CESR. We also report first results from our efforts to model these lines by ab initio Monte Carlo simulation.

Key words. line: identification – instrumentation: miscellaneous – methods: data analysis – methods: numerical

1. Introduction

The Spectrometer for INTEGRAL (SPI) is one of the two main instruments on board ESA's INTEGRAL observatory launched from Baikonour, Kazakhstan, on Oct. 17, 2002. The INTEGRAL mission was placed into a highly elliptical orbit with a perigee of 9000 km. Consequently, INTEGRAL does not benefit from geomagnetic shielding and is fully exposed to all cosmic rays. Interactions of these cosmic rays within the instrument and spacecraft materials are the dominant source of instrumental background for SPI. In particular, delayed decays of radio-isotopes and prompt de-excitations of excited nuclei produced in nuclear interactions give rise to a plethora of instrumental lines which are the focus of this work. The general characteristics of the SPI instrumental background and its temporal and orbital variation are described by Jean et al. (2003).

A detailed understanding of the instrumental lines is valuable for both the operation of the instrument as well as for scientific analyses. Accurate line identifications are a prerequisite for the absolute energy calibration of the detectors and the monitoring of their radiation damage. Many scientific analyses, in particular studies of diffuse gamma-ray emission from the Galaxy, necessitate modelling both the amplitude and shape of the instrumental background in specific energy regions. Typically, this involves modelling of instrumental lines.

Send offprint requests to: G. Weidenspointner,
e-mail: Georg.Weidenspointner@cesr.fr

⋆ Based on observations with INTEGRAL, an ESA project with instruments and science data centre funded by ESA member states (especially the PI countries: Denmark, France, Germany, Italy, Switzerland, Spain), Czech Republic and Poland, and with the participation of Russia and the USA.

⋆⋆ Table 1 is only available in electronic form at
http://www.edpsciences.org

⋆⋆⋆ *Present address:* Centre d'Étude Spatiale des Rayonnements, 9 avenue Colonel Roche, BP 4346, 31028 Toulouse Cedex 4, France.

2. Instrument description and data analysis

The SPI spectrometer consists of an array of 19 actively cooled high resolution Ge detectors with a total volume of 3396 cm^3. The detectors cover an energy range of 20–8000 keV at an energy resolution of about 2.5 keV full width at half maximum (FHWM) at 1.1 MeV. SPI employs an active anti-coincidence shield made of bismuth germanate (BGO), which also acts as a collimator. Detailed descriptions of the instrument, its ground

calibration, and in-flight performance are given by Vedrenne et al. (2003); Attié et al. (2003); Roques et al. (2003).

The data used in this investigation were recorded in March 2003 (i.e. during revolutions 49, 50, 51, and 53). During this time the variation of the temperature of the Ge detectors and their electronics, and consequently the gain drift, was sufficiently small to allow us to use a single energy calibration for the combined data. Also, these revolutions followed shortly after the first detector annealing, hence the energy resolution of the detectors was close to optimal (see Roques et al. 2003). An absolute energy calibration was obtained by first summing all data for each detector and by assuming a quadratic relation between channel number and energy for both the low (up to about 2 MeV) and high gain range (above about 2 MeV). We found this calibration to be accurate to within about 0.2 keV for most energies, and slightly less accurate at the lowest (below about 200 keV) and the highest (above a few MeV) energies. All fits were performed using the GASPAN[1] gamma spectrum analysis program. We found that a Gaussian, with its width constrained at the instrumental resolution, provided an adequate description of the line shape at all energies.

The event types used in this study consist of single detector events (events that deposited energy in only one detector), double and triple events (events that involve coincident interactions in two or three detectors), and so-called broken double events (the energy deposits in individual detectors for double events). A detailed description of the various SPI event types is given in Roques et al. (2003), Vedrenne et al. (2003).

3. Line identifications and characteristics

The analysis and identification of the more than 300 instrumental lines and spectral features is an on-going process; Table 1 summarizes our current knowledge. An electronic version of the table, which will continuously be updated as our understanding advances, is available at CESR[2]. Up to 8 MeV the table entries refer to single detector events[3]. Combining coincident energy deposits in multiple detectors allows us to observe lines above 8 MeV. The quoted line count rates represent the sum over the full detector array.

Table 1 is organized in five columns. The first two columns provide energy and count rate of the observed line or spectral feature; the quoted errors are statistical only. Columns three and four provide, if possible, the identified parent process and the nominal energy of the line or feature based on evaluated nuclear data available at the Brookhaven National Laboratory[4] and, in addition for lines from (n, γ) reactions, on Frankle et al. (2001); Reedy & Frankle (2002). The comments in column five are intended to provide supplementary information.

We have not applied a strict and uniform criterion on the statistical significance of lines for inclusion in the table. For unidentified features, indicated by question marks in columns three and four, the significance is about 5σ. However, if we have reason to believe in the reality of a weak line or feature based on identified stronger lines and known branching ratios, then these are listed as well. If we have reason to believe that multiple processes contribute to a single line or feature, then these are listed in the order of their (suspected) contribution. In some cases we suspect a yet unidentified partial contribution to a line, which we again indicate with question marks. The measured line energy and rate are listed only for the first contributor.

Despite the excellent energy resolution of SPI there are many regions in the spectrum where a few or even several closely spaced lines blend to form a broad line or feature, or where lines and instrinsically broad features merge. These regions are indicated in the table. In particular for complex features it can be very difficult to determine reliable values for contributing lines. At this early stage of the analysis we then limit ourselves to merely listing identified contributors, without quoting values in the first two columns. Especially for complex regions the list of contributors can *not* assumed to be exhaustive.

We followed a variety of approaches to arrive at the line identifications in Table 1. All identifications required close agreement between the measured energy and the nominal energy of the parent process. Processes involving proton and neutron interactions had to be plausible considering the material composition of instrument and spacecraft and the particle fluxes and cross-sections. The Monte Carlo simulations described in Sect. 4 were particularly helpful in this respect. For decays that result in the emission of multiple photons consistency was required between observed and expected line ratios. Again, Monte Carlo simulations were very helpful, especially for decays within or close to the veto shield or the Ge detectors. We also consulted compilations of instrumental lines seen in other high resolution Ge spectrometers flown in space, such as on HEAO-3 (Wheaton et al. 1989), the TGRS on board WIND (Weidenspointner et al. 2003), and on Mars Odyssey (Evans et al. 2002), as well as on balloons such as GRIS (Bartlett 1994) and HIREGS (Feffer 1996).

The strength of some of the listed lines varies with time; the quoted values represent an average for March 2003. For lines from prompt de-excitations or the decay of short-lived isotopes the main cause for time variability is the variation of the ambient cosmic radiation. For lines from the decay of long-lived isotopes the variability of the line strength is mainly due to the interplay of activation and radioactive decay. This should be taken into consideration when trying to predict line strengths in the future. Also, there can be significant differences in the line strength between individual detectors (see Jean et al. 2003, for more details on background variations).

A particularly abrupt change in the ambient radiation environment occurs during times when INTEGRAL is exposed

[1] The software, developed by F. Riess, and documentation are available under `http://ftp.leo.org/download/pub/science/physics/software/gaspan/`

[2] `http://sigma-2.cesr.fr/spi/download/spi_intrumental_lines/`

[3] In 1.4–1.6 MeV only single detector events that also triggered the PSD electronics have been used to avoid electronic noise; the count rates were corrected for the efficiency of the PSD electronics which at these energies is about 85% (see Roques et al. 2003).

[4] `http://www.nndc.bnl.gov/`

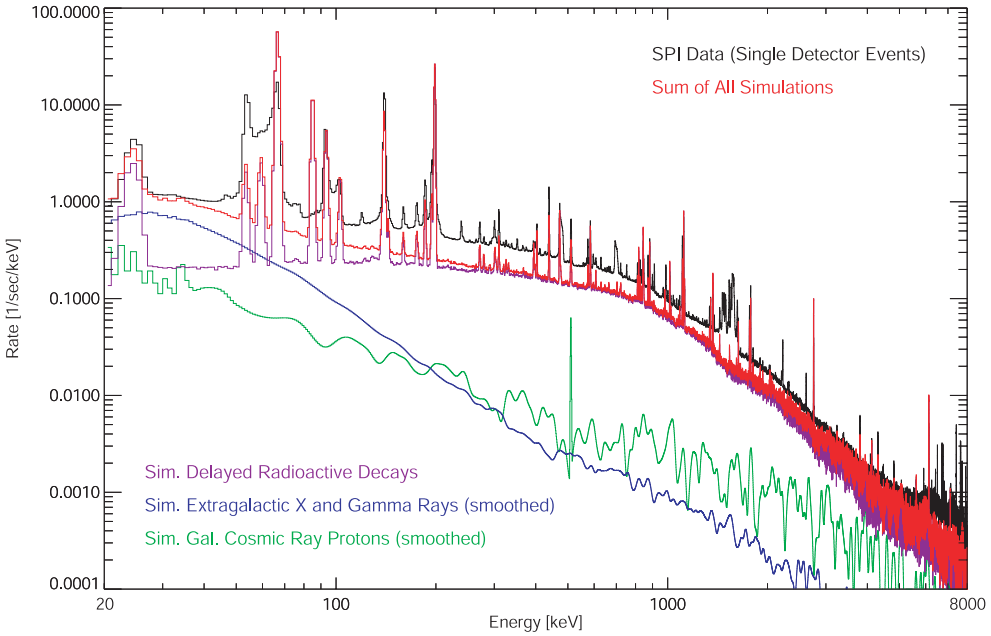

Fig. 1. A comparison of simulated SPI single detector events with actual flight data. Details are given in the text. The broad spikes in the data in 1.4–1.6 MeV are electronic noise.

to solar energetic particles. Regarding the SPI background lines, the most important effect of solar energetic particles is to greatly increase the strengths of lines due to inelastic proton scattering (e.g. on Al and C). In some cases lines which are too weak in the "quiescent" background become detectable during a solar event. The time variation of these lines follows closely the intensity of the solar proton flux. A more detailed discussion of the effect of solar energetic particles on the background of SPI is beyond the scope of this paper and will be presented elsewhere (see also Jean et al. 2003).

An important part of the background lines arises from decays of isomers or from EC decays of radio-isotopes produced by spallation and neutron capture reactions *inside* the Ge crystals. In general, an isomer decays by internal transition to its ground state and produces a single background line. However, if the half-life of an isomeric level is similar to the peaking time τ of the electronic, which for SPI is about 8 μs, and if the isomeric level is part of a cascade, then this cascade gives rise to a double-horn structure in the spectrum. For SPI this is the case for ^{67m}Zn and ^{73m}Ge inside the Ge detectors. The interpeak region is due to an electronic effect which results in a partial summation of two energy deposits that are about τ apart in time. The detailed dependence of the double-horn shape on the electronic time constants and the de-excitation cascade is complicated. Gamma-ray transitions in the daughter nucleus following EC decay inside the Ge crystals appear at two distinct energies, depending on the shell from which the electron was captured and on whether the gamma ray and electron binding energies are summed. The first EC feature is a blend of two components: gamma rays at the nominal transition energy[5], and gamma rays summed with the electron binding energy for captures from above the K shell (labelled ^{AA}ZZ(EC) + L in the table). The proportion of the different contributions is difficult to estimate. The second EC feature (labelled ^{AA}ZZ(EC) + K) is from K-shell capture in the crystal detecting the gamma ray, the energy of the gamma ray line being shifted by the K-shell electron binding energy.

Above 5 MeV, with the exception of the ^{16}N(β^-)^{16}O decay and ^{16}O* line, all lines are due to capture reactions of low energy neutrons in the Ge crystals or surrounding material. The positions and widths of these lines suggest that they were produced by capture of thermal neutrons.

4. Background modelling

We employed the MGGPOD suite in an attempt to model the SPI instrumental background, in particular the many gamma ray lines, by Monte Carlo simulation. In a nutshell, the MGGPOD suite was developed to simulate ab initio the physical processes relevant for the production of instrumental backgrounds. These include the build-up and delayed decay of radioactive isotopes as well as the prompt de-excitation of excited nuclei, both of which give rise to a plethora of instrumental gamma-ray background lines in addition to continuum backgrounds. A detailed description of the MGGPOD suite can be found in Weidenspointner et al. (2003).

A Monte Carlo simulation of instrumental backgrounds requires a mathematical representation of the instrumental set-up (the so-called mass model) and a model of the radiation environment. In our simulation we combined the very detailed mass model of the SPI instrument developed at NASA/GSFC (see Sturner et al. 2003) with "The INTEGRAL Mass Model" (TIMM) developed at the University of Southampton (Ferguson et al. 2003) which describes the spacecraft and the other instruments on board. The radiation environment consisted of two components: the cosmic X and gamma radiation was modelled according to Gruber et al. (1999); the Galactic cosmic-ray proton spectrum, corrected for solar modulation, was based on the models of Moskalenko et al. (2002).

A comparison of a MGGPOD simulation of SPI single detector events with actual flight data (an empty field observation during Rev. 13) is depicted in Fig. 1. It has to be

[5] ECs outside the detectors contribute as well.

emphasized that in this simulation the PROMPT package, which in the framework of MGGPOD is used for modelling prompt gamma-ray line emission after spallation, neutron capture, and inelastic neutron scattering (see Weidenspointner et al. 2003), has *not* been included. The simulation comprises three background components: background events due to extragalactic X and gamma rays (blue), prompt background events resulting from nuclear interactions of cosmic-ray protons in spacecraft and instrument (green), and background events that arise from the delayed radioactive decay of radio-isotopes produced in nuclear interactions of cosmic-ray protons and their hadronic secondaries (purple). The sum of these three components is depicted in red; the actual flight data are represented by the black spectrum. A similar comparison between a simulated background spectrum, obtained with the GGOD Monte Carlo suite, and SPI data is shown in Ferguson et al. (2003).

As can be seen in Fig. 1, the MGGPOD simulation reproduces well the overall shape and magnitude of the continuum background, and also reproduces well many lines from radioactive decays. Special attention has been given to the numerous lines that result from decays involving isomeric levels, particularly in the Ge detectors. The simulation accounts for 71% of the observed total 20–8000 keV count rate. Below 4 MeV the simulation never falls short of the data by more than a factor of 2. At higher energies, where gamma rays from (thermal) neutron capture are important, but not yet included in the simulation, the difference can be larger. The lines from radioactive decays which are produced in the simulation provided very useful information for our line identification efforts (see Sect. 3). Modelling the SPI instrumental background by Monte Carlo simulation is an ongoing effort. A more detailed description and comparison will be presented in a forthcoming publication.

5. Discussion

SPI employs a large Ge detector array with a massive BGO anti-coincidence shield on board a heavy spacecraft. The confluence of these factors results in an instrumental background that is very rich in lines and spectral features for which we provide first identifications. The main contributor to this background, both line and continuum, are radioactive decays, particularly within the Ge crystals, nearby materials, and the BGO shield. Spallation and neutron activation are the dominant source of activation, as has been found for previous Ge spectrometers (see e.g. Wheaton et al. 1989; Evans et al. 2002). These decays are well reproduced by ab initio Monte Carlo simulation using the MGGPOD suite. Thermal neutron capture is responsible for numerous and strong lines at several MeV; their unexpected presence poses a difficult challenge for our physical understanding of instrumental backgrounds and for Monte Carlo codes such as MGGPOD. Both the analysis and identification as well as the modelling of the line background are work in progress. We expect to present more detailed results in the future.

Acknowledgements. The SPI project has been completed under the responsibility and leadership of CNES. We are grateful to ASI, CEA, CNES, DLR, ESA, INTA, NASA and UCL for their support.

References

Attié, D., Cordier, B., Gros, M., et al. 2003, 411, L71
Bartlett, L. M. 1994, Ph.D. Thesis, University of Maryland, USA
Diehl, R., Baby, N., Beckmann, V., et al. 2003, 411, L117
Evans, L. G., Boynton, W. V., Reedy, R. C., et al. 2002, Proc. of SPIE 4784, X-Ray and Gamma-Ray Detectors and Applications IV, 31
Feffer, P. T. 1996, Ph.D. Thesis, University of California Berkeley, CA 94720, USA
Ferguson, C., Barlow, E. J., Bird, A. J., et al. 2003, 411, L19
Frankle, S. C., Reedy, R. C., & Young, P. G. 2001, LANL Report LA-13812
Gruber, D. E., Matteson, J. L., Peterson, L. E., & Jung, G. V. 1999, ApJ, 520, 124
Jean, P., Vedrenne, G., Roques, J.-P., et al. 2003, 411, L107
Moskalenko, I. V., Strong, A. W., Ormes, J. F., & Potgieter, M. S. 2002, ApJ, 565, 280
Reedy, R. C., & Frankle, S. C. 2002, Atomic Data and Nuclear Tables, 80, 1
Roques, J.-P., Schanne, S., von Kienlin, A., et al. 2003,411, L91
Sturner, S. J., Shrader, C. R., Weidenspointner, G., et al. 2003, 411, L81
Vedrenne, G., Roques, J.-P., Schönfelder, V., et al. 2003, 411, L63
Weidenspointner, G., et al. 2003, in preparation
Wheaton, W. A., Jacobson, A. S., Ling, J. C., Mahoney, W. A., & Varnell, L. S. 1989, in High-Energy Radiation Background in Space (AIP 186), 304

Online Material

Table 1. SPI instrumental lines.

Measured		Parent	Nominal	Comment
Energy [keV]	Count rate [cts/sec]	process	energy [keV]	
23.726(4)	3.44(2)	^{71m}Ge(IT)^{71}Ge	23.438(15)	blend
25.153(2)	6.23(2)	^{58m}Co(IT)^{58}Co	24.889(21)	blend
26.6(1)	0.10(1)	^{72}Zn(β^-)^{72}Ga	26.8(3)	weak, blend
46.92(1)	0.357(1)	^{210}Pb(β^-)^{210}Bi	46.5390(10)	^{238}U series
~53–67		^{73m}Ge(IT)^{73}Ge	53.440(9)	^{73m}Ge complex
		^{60m}Co(IT)^{60}Co	58.603(7)	^{73m}Ge complex
		^{74m}Ga(IT)^{74}Ga	59.7	^{73m}Ge complex, sum peak
		^{73m}Ge(IT)^{73}Ge	66.725(9)	^{73m}Ge complex, sum peak
75.13(1)	0.368(8)	Bi $K_{\alpha 2}$ X-ray	74.8	various isotopes
		Pb $K_{\alpha 1}$ X-ray	75.0	various isotopes
77.304(7)	0.496(9)	Bi $K_{\alpha 1}$ X-ray	77.1	various isotopes
84.50(3)	0.075(9)	?	?	
		^{68m}Cu(IT)^{68}Cu	84.6(4)	
87.31(2)	0.41(1)	Bi $K_{\beta 1}$ X-ray	87.3	various isotopes
~91–105		^{67}Ga(EC)^{67}Zn	91.266(5)	^{67m}Zn complex
		^{67}Ga(EC)^{67}Zn + L	92.4	^{67m}Zn complex
		^{67m}Zn(IT)^{67}Zn	93.311(5)	^{67m}Zn complex
		^{67}Ga(EC)^{67m}Zn(IT)^{67}Zn + L	94.4	^{67m}Zn complex
		^{67}Ga(EC)^{67}Zn + K	100.93(1)	^{67m}Zn complex
		^{67}Ga(EC)^{67m}Zn(IT)^{67}Zn + K	102.880(5)	^{67m}Zn complex
109.6(1)	0.020(3)	^{19}F*	109.894(5)	
112.9(1)	0.023(3)	?	?	
116.6(2)	0.018(4)	^{65}Ga(EC)^{65}Zn	115.09(4)	
		^{65}Ga(EC)^{65}Zn + L	116.2	
119.689(7)	0.441(5)	^{72}Zn(β^-)^{72}Ga	119.54(34)	sum peak
		^{72m}Ga(IT)^{72}Ga	119.54(34)	sum peak
122.15(3)	0.132(4)	^{57}Co(EC)^{57}Fe	122.0614(4)	
		^{57}Co(EC)^{57}Fe + L	122.9	
124.84(5)	0.057(4)	^{65}Ga(EC)^{65}Zn + K	124.76(1)	
129.6(1)	0.020(3)	^{57}Co(EC)^{57}Fe + K	129.1734(4)	
~132–140		^{57}Co(EC)^{57}Fe	136.4743(5)	^{75m}Ge complex
		^{57}Co(EC)^{57}Fe + L	137.3	^{75m}Ge complex
139.945(1)	30.26(5)	^{75m}Ge(IT)^{75}Ge	139.68(3)	^{75m}Ge complex
~140–147		^{57}Co(EC)^{57}Fe + K	143.586(1)	^{75m}Ge complex
		^{46m}Sc(IT)^{46}Sc	142.528(8)	^{75m}Ge complex
		^{72}Zn(β^-)^{72}Ga	144.7(1)	^{75m}Ge complex
159.735(8)	0.801(8)	^{47}Sc(β^-)^{47}Ti	159.377(12)	
		^{77m}Ge(IT)^{77}Ge	159.7(1)	
162.78(2)	0.124(3)	?	?	
175.10(1)	1.06(1)	^{71}As(EC)^{71}Ge	174.949(4)	blend
		^{71m}Ge(IT)^{71}Ge	174.949(4)	
		^{70}Ge(n, γ)^{71}Ge	174.949(4)	
176.8(2)	0.17(2)	^{71}As(EC)^{71}Ge + L	176.3	blend
184.65(2)	0.72(1)	^{67}Ga(EC)^{67}Zn	184.577(10)	blend
		^{67}Cu(β^-)^{67}Zn	184.577(10)	
185.97(1)	2.16(4)	^{71}As(EC)^{71}Ge + K	186.057(5)	blend
		^{67}Ga(EC)^{67}Zn + L	185.7	
~190–198		^{67}Ga(EC)^{67}Zn + K	194.236(1)	^{71m}Ge complex
198.368(1)	52.63(4)	^{71m}Ge(IT)^{71}Ge	198.392(16)	^{71m}Ge complex, sum peak
~198–215		^{72}Zn(β^-)^{72}Ga	208.45(5)	^{71m}Ge complex, sum peak
		^{77}Ge(β^-)^{77}As	211.03(3)	^{71m}Ge complex
238.708(6)	0.499(4)	^{212}Pb(β^-)^{212}Bi	238.632(2)	blend, ^{232}Th series
		^{19}Ne*	238.3	

Table 1. continued.

Measured		Parent	Nominal	Comment
Energy [keV]	Count rate [cts/sec]	process	energy [keV]	
241.53(3)	0.084(3)	^{214}Pb(β^-)^{214}Bi	241.997(3)	blend, ^{238}U series
		^{55}Cr*	241.94(5)	
253.05(4)	0.063(3)	?	?	
257.5(1)	0.021(3)	?	?	
		^{234m}Pa(β^-)^{234}U	258.26(10)	^{238}U series
264.64(3)	0.094(3)	^{77}Ge(β^-)^{77}As	264.44(3)	
		^{77}As*	264.44(3)	
271.257(5)	0.558(5)	^{44m}Sc(IT)^{44}Sc	270.9(2)	
279.21(1)	0.171(5)	^{203}Pb(EC)^{203}Tl	279.1967(12)	
283.2(1)	0.1714(4)	?	?	
		^{61}Cu(EC)^{61}Ni	282.956(2)	
		^{61}Cu(EC)^{61}Ni + L	283.9	
291.23(3)	0.070(3)	^{61}Cu(EC)^{61}Ni + K	291.289(2)	complex
295.30(3)	0.112(4)	^{214}Pb(β^-)^{214}Bi	295.224(2)	complex, ^{238}U series
297.40(2)	0.156(4)	^{73}Ga(β^-)^{73}Ge	297.32(5)	complex
300.24(2)	0.59(1)	^{67}Ga(EC)^{67m}Zn	300.219(10)	complex
		^{212}Pb(β^-)^{212}Bi		complex, ^{232}Th series, weak
301.55(6)	0.144(9)	^{67}Ga(EC)^{67m}Zn + L	301.3	complex
		^{212}Pb(β^-)^{212}Bi	300.087(10)	complex, ^{232}Th series
303.87(2)	0.154(5)	^{75m}As(IT)^{75}As	303.9236(10)	complex
309.873(5)	1.207(9)	^{67}Ga(EC)^{67m}Zn + K	309.878(10)	blend
311.9(1)	0.060(4)	?	?	blend
320.09(2)	0.119(3)	^{51}Cr(EC)^{51}V	320.0824(4)	
		^{51}Cr(EC)^{51}V + L	320.7	
		^{51}Ti(β^-)^{51}V	320.0824(4)	weak
325.66(1)	0.195(3)	^{51}Cr(EC)^{51}V + K	325.5475(4)	blend
		^{73}Ga(β^-)^{73}Ge	325.70(7)	blend
328.4(1)	0.019(2)	?	?	blend
331.14(3)	0.085(3)	^{201}Pb(EC)^{201}Tl	331.19(3)	blend
338.22(2)	0.101(3)	^{228}Ac(β^-)^{228}Th	338.320(3)	^{232}Th series
343.5(1)	0.019(2)	^{175}Hf(EC)^{175}Lu	343.40(8)	
		^{206}Bi(EC)^{206}Pb	343.51(3)	weak
351.0(1)	0.07(2)	^{21}F(β^-)^{21}Ne	350.72(6)	blend
352.0(1)	0.17(2)	^{214}Pb(β^-)^{214}Bi	351.932(2)	blend, ^{238}U series
360.6(2)	0.014(2)	^{181}Re(EC)^{181}W	360.7(3)	
365.62(3)	0.102(3)	^{181}Re(EC)^{181}W	365.5(3)	blend
367.80(5)	0.061(3)	^{200}Tl(EC)^{200}Hg	367.942(10)	blend
372.6(3)	0.012(3)	^{43}K(β^-)^{43}Ca	372.760(7)	blend
		^{43}Sc(EC)^{43}Ca	372.760(7)	blend
		^{43}Sc(EC)^{43}Ca + L	373.2	blend
374.78(3)	0.095(4)	^{204}Bi(EC)^{204}Pb	374.76(7)	blend
		^{204m}Pb(IT)^{204}Pb	374.76(7)	blend
		^{43}Sc(EC)^{43}Ca + L	376.8	blend, weak
381.4(2)	0.012(2)	?	?	blend
		^{66}Ge(EC)^{66}Ga	381.85(5)	blend
383.6(2)	0.016(3)	^{195}Pb(EC)^{195}Tl	383.64(12)	blend
		^{195m}Tl(IT)^{195}Tl	383.64(12)	blend
		^{66}Ge(EC)^{66}Ga + L	383.1	blend
390.1(2)	0.017(3)	^{25}Na(β^-)^{25}Mg	389.7	complex
392.3(2)	0.07(1)	^{66}Ge(EC)^{66}Ga + K	392.22(5)	complex
393.75(9)	0.210(8)	^{67}Ga(EC)^{67}Zn	393.5(1)	complex
		^{67}Ga(EC)^{67}Zn + L	394.6	complex
395.3(1)	0.071(8)	?	?	complex
397.98(2)	0.251(3)	?	?	complex
		^{206}Bi(EC)^{206}Pb	398.00(3)	weak, complex
400.47(5)	0.082(3)	?	?	complex
403.058(5)	0.796(5)	^{67}Ga(EC)^{67}Zn + K	403.188(10)	complex

Table 1. continued.

Measured		Parent	Nominal	Comment
Energy [keV]	Count rate [cts/sec]	process	energy [keV]	
411.78(2)	0.122(3)	?	?	
		^{198}Au(β^-)^{198}Hg	411.8020(2)	
425.29(7)	0.045(3)	?	?	
427.92(4)	0.073(3)	^{73m}As(IT)^{73}As	427.83(10)	
436.9(2)	0.08(1)	?	?	blend
438.619(5)	2.75(3)	^{69m}Zn(IT)^{69}Zn	438.634(18)	blend
440.4(1)	0.09(1)	^{23}Ne(β^-)^{23}Na	439.991(10)	blend
442.5(2)	0.017(3)	?	?	blend
455.3(1)	0.05(1)	?	?	
~470–485		^{24m}Na(IT)^{24}Na	472.202(9)	complex
		^{10}B(n,$\alpha\gamma$)^{7}Li	477.6	complex, kinematically broadened
		^{77}Ge(β^-)^{77}As	475.43(3)	complex
		^{7}Be(EC)^{7}Li	477.595(3)	complex
497.0(2)	0.023(7)	?	?	
		^{206}Bi(EC)^{206}Pb	497.06(4)	
499.92(7)	0.037(7)	^{70}Ge(n, γ)^{71}Ge	499.876(10)	
		^{71}As(EC)^{71}Ge	499.876(10)	
510.948(6)	1.73(1)	positron annihilation	511.0	kinematically broadened
		many sources		
538.5(2)	0.011(2)	?	?	
		^{66}Ge(EC)^{66}Ga	536.74(7)	
		^{66}Ge(EC)^{66}Ga + L	537.9	
		^{206}Bi(EC)^{206}Pb	537.45(4)	
547.7(1)	0.021(2)	?	?	
		^{66}Ge(EC)^{66}Ga	547.11(7)	
555.6(1)	0.032(3)	?	?	blend
557.4(1)	0.040(3)	?	?	blend
563.39(5)	0.043(2)	^{76}Ge(n,n')	562.93(3)	saw tooth
		^{52}Cr(n, γ)^{53}Cr	564.0	
569.69(2)	0.110(4)	^{207}Bi(EC)^{207}Pb	569.702(2)	
		^{207m}Pb(IT)^{207}Pb	569.702(2)	
574.25(5)	0.44(3)	^{69}Ge(EC)^{69}Ga	574.17(3)	blend
575.5(1)	0.10(2)	^{69}Ge(EC)^{69}Ga + L	575.4	blend
580.2(1)	0.033(3)	^{205}Bi(EC)^{205}Pb	579.8	
		^{200}Tl(EC)^{200}Hg	579.28(9)	weak
582.4(2)	0.043(4)	?	?	blend
		^{208}Tl(β^-)^{208}Pb	583.191(2)	blend, natural radioactivity
584.558(5)	1.051(7)	^{69}Ge(EC)^{69}Ga + K	584.54(3)	blend
~596–610		^{74}Ge(n,n')	596.847(6)	^{74}Ge(n,n') complex, saw tooth
		^{73}Ge(n, γ)^{74}Ge	595.847(6)	^{74}Ge(n,n') complex
		^{74}As(EC)^{74}Ge + L	597.1	^{74}Ge(n,n') complex
		^{214}Bi(EC)^{214}Po	609.312(7)	^{74}Ge(n,n') complex, ^{238}U series
		^{74}As(EC)^{74}Ge + K	606.950(6)	^{74}Ge(n,n') complex
616.9(1)	0.0213(2)	?	?	
		^{43}K(β^-)^{43}Ca	617.490(6)	
628.94(1)	0.181(3)	^{201m}Pb(IT)^{201}Pb	629.1(2)	
639.5(2)	0.015(2)	?	?	blend
641.9(2)	0.014(2)	?	?	blend
646.37(4)	0.064(3)	?	?	
650.3(1)	0.015(2)	?	?	
656.0(1)	0.033(4)	^{61}Cu(EC)^{61}Ni	656.008(4)	blend
		^{61}Cu(EC)^{61}Ni + L	657.0	blend
657.7(1)	0.049(5)	?	?	blend
661.6(3)	0.009(2)	^{181}Re(EC)^{181}W	661.8(4)	
664.32(4)	0.076(3)	^{61}Cu(EC)^{61}Ni + K	664.341(4)	
671.25(3)	0.070(2)	^{38m}Cl(IT)^{38}Cl	671.361(8)	
~693–705		^{72}Ge(n,n')	689.6(5)	^{72}Ge(n,n') complex, saw tooth
		^{205}Bi(EC)^{205}Pb	703.44(3)	^{72}Ge(n,n') complex

Table 1. continued.

Measured		Parent	Nominal	Comment
Energy [keV]	Count rate [cts/sec]	process	energy [keV]	
721.16(1)	0.156(2)	^{68m}Cu(IT)^{68}Cu	721.6(7)	sum peak
		^{203}Bi(EC)^{203}Pb	722.4(4)	
727.31(6)	0.032(2)	^{212}Bi(β^-)^{212}Po	727.330(9)	^{232}Th series
739.7(1)	0.024(2)	?	?	
743.25(8)	0.025(2)	?	?	
		^{234m}Pa(β^-)^{234}U	742.81(3)	^{238}U series
748.6(2)	0.015(2)	?	?	blend
751.96(1)	0.198(2)	^{204m}Bi(IT)^{204}Bi	752.1(2)	blend
755.7(2)	0.010(2)	?	?	blend
766.12(5)	0.054(3)	^{234m}Pa(β^-)^{234}U	766.38(2)	^{238}U series
785.9(3)	0.008(2)	^{214}Pb(β^-)^{214}Bi	785.96(9)	^{238}U series
		^{234m}Pa(β^-)^{234}U	786.27(3)	^{238}U series
803.3(2)	0.011(2)	^{206}Bi(EC)^{206}Pb	803.06(3)	
808.2(2)	0.016(2)			blend
810.881(5)	0.613(3)	^{58}Co(EC)^{58}Fe	810.775(9)	blend
		^{58}Co(EC)^{58}Fe + L	811.6	blend
814.02(8)	0.028(2)	?	?	blend
817.878(5)	0.754(3)	^{58}Co(EC)^{58}Fe + K	817.887(9)	blend
820.48(7)	0.040(2)	^{203}Bi(EC)^{203}Pb	820.3(3)	blend
825.17(1)	0.288(2)	^{203m}Pb(IT)^{203}Pb	825.2(1)	blend
		^{203}Bi(EC)^{203}Pb	825.2(1)	blend
827.8(2)	0.011(3)	?	?	blend
		^{200}Tl(EC)^{200}Hg	828.32(10)	
834.88(2)	0.350(5)	^{54}Mn(EC)^{54}Cr	834.848(3)	blend
		^{54}Mn(EC)^{54}Cr + L	835.4	blend
837.93(8)	0.034(2)	?	?	blend
840.81(1)	0.229(2)	^{54}Mn(EC)^{54}Cr + K	840.837(3)	complex
843.822(5)	0.740(3)	^{27}Mg(β^-)^{27}Al	843.74(3)	complex
846.794(9)	0.346(2)	^{56}Mn(β^-)^{56}Fe	846.771(5)	complex
		^{56}Co(EC)^{56}Fe	846.771(5)	complex
		^{56}Co(EC)^{56}Fe + L	847.6	complex
849.9(1)	0.022(2)	?	?	complex
853.00(4)	0.005(2)	^{56}Co(EC)^{56}Fe + K	853.88(5)	complex
860.9(3)	0.007(2)	^{208}Tl(β^-)^{208}Pb	860.564(5)	natural radioactivity
872.28(2)	0.42(1)	^{69}Ge(EC)^{69}Ga	872.14(3)	blend
		^{69}Ge(EC)^{69}Ga + L	873.3	blend
874.1(2)	0.039(8)	?	?	blend
880.9(3)	0.04(1)	^{206}Bi(EC)^{206}Pb	880.98(5)	blend
882.52(2)	0.744(1)	^{69}Ge(EC)^{69}Ga + K	882.51(3)	blend
889.41(7)	0.030(2)	^{46}Sc(β^-)^{46}Ti	889.277(3)	
		^{67}Ga(EC)^{67}Zn	887.693(15)	weak
		^{67}Ga(EC)^{67}Zn + L	888.8	weak
896.45(8)	0.032(2)	^{203}Bi(EC)^{203}Pb	896.9(4)	blend
		^{206}Bi(EC)^{206}Pb	895.12(5)	blend
		^{67}Ga(EC)^{67}Zn + K	894.351(15)	blend, weak
899.17(1)	0.205(2)	^{204}Bi(EC)^{204}Pb	899.15(3)	blend
		^{204m}Pb(IT)^{204}Pb	899.15(3)	blend
903.3(2)	0.010(2)	?	?	
908.88(6)	0.047(2)	?	?	blend
		^{61}Cu(EC)^{61}Ni	908.631(17)	blend, weak
		^{61}Cu(EC)^{61}Ni + L	909.5	blend, weak
911.40(1)	0.315(3)	^{228}Ac(β^-)^{228}Th	911.204(4)	blend, ^{232}Th series
916.8(2)	0.008(2)	^{61}Cu(EC)^{61}Ni + K	916.963(17)	
920.9(1)	0.014(2)	?	?	
932.1(2)	0.007(1)	?	?	
935.7(3)	0.007(2)	^{52}Mn(EC)^{52}Cr	935.538(11)	
961.5(5)	0.013(1)	^{73}Ge(n, γ)^{74}Ge	961.1	
964.9(1)	0.017(1)	^{228}Ac(β^-)^{228}Th	964.766(10)	^{232}Th series
969.05(2)	0.080(2)	^{228}Ac(β^-)^{228}Th	968.971(17)	^{232}Th series

Table 1. continued.

Measured		Parent	Nominal	Comment
Energy [keV]	Count rate [cts/sec]	process	energy [keV]	
974.85(7)	0.0243(1)	^{25}Na(β^-)^{25}Mg	974.72	
983.80(3)	0.064(2)	^{48}V(EC)^{48}Ti	983.517(5)	blend
		^{48}Sc(β^-)^{48}Ti	983.517(5)	blend
		^{48}V(EC)^{48}Ti + L	984.2	blend
		^{204}Bi(EC)^{204}Pb	983.98(3)	blend
987.595(6)	0.384(2)	^{205m}Pb(IT)^{205}Pb	987.62(3)	blend
		^{48}V(EC)^{48}Ti + K	988.702(5)	blend
991.96(6)	0.029(2)	?	?	
1001.14(2)	0.068(2)	^{234m}Pa(β^-)^{234}U	1001.03(3)	^{238}U series
1014.485(7)	0.283(2)	^{27}Mg(β^-)^{27}Al	1014.42(3)	
		^{205m}Pb(IT)^{205}Pb	1013.84(3)	
1021.96(3)	0.067(2)	positron annihilation	1022.0	
		many sources		
1026.3(1)	0.013(1)	?	?	
1037.9(4)	0.010(4)	^{48}Sc(β^-)^{48}Ti	1037.599(26)	blend
1039.49(7)	0.057(4)	^{66}Ga(EC)^{66}Zn	1039.237(3)	blend
		^{70}Ge(n,n')	1039.20(8)	blend, saw tooth
		^{66}Ga(EC)^{66}Zn + L	1040.3	blend
1044.4(2)	0.009(2)	?	?	
1048.94(5)	0.040(2)	^{66}Ga(EC)^{66}Zn + K	1048.896(3)	
1063.75(3)	0.067(2)	^{207m}Pb(IT)^{207}Pb	1063.662(4)	
1077.59(3)	0.062(2)	^{68}Ga(EC)^{68}Zn	1077.34(5)	
		^{68}Ga(EC)^{68}Zn + L	1078.4	
1087.09(2)	0.097(2)	^{68}Ga(EC)^{68}Zn + K	1087.00(5)	
1095.7(3)	0.006(1)	?	?	
1106.98(3)	0.92(4)	^{69}Ge(EC)^{69}Ga	1107.01(6)	blend
1108.36(7)	0.17(3)	^{69}Ge(EC)^{69}Ga + L	1108.2	blend
1115.46(2)	0.353(8)	^{65}Zn(EC)^{65}Cu	1115.546(4)	blend
		^{65}Zn(EC)^{65}Cu + L	1116.5	blend
1117.257(6)	1.79(1)	^{69}Ge(EC)^{69}Ga + K	1117.38(6)	blend
1120.87(2)	0.112(3)	^{214}Bi(EC)^{214}Po	1120.287(10)	blend, ^{238}U series
		^{46}Sc(β^-)^{46}Ti	1120.545(4)	blend
		^{182}Ta(β^-)^{182}W	1121.3008(17)	blend
1124.513(4)	0.545(3)	^{65}Zn(EC)^{65}Cu + K	1124.525(4)	
1139.3(2)	0.011(1)	?	?	
1157.08(7)	0.024(1)	^{44}Sc(EC)^{44}Ca	1157.020(15)	
1161.2(2)	0.009(1)	?	?	
1172.9(2)	0.009(1)	^{60}Co(β^-)^{60}Ni	1173.228(3)	
1185.6(2)	0.009(1)	^{61}Cu(EC)^{61}Ni	1185.234(15)	
		^{61}Cu(EC)^{61}Ni + L	1186.2	
1189.40(6)	0.031(1)	^{182}Ta(β^-)^{182}W	1189.0503(17)	
		^{205}Bi(EC)^{205}Pb	1190.03(4)	
1193.6(1)	0.018(1)	^{61}Cu(EC)^{61}Ni + K	1193.57(2)	
1204.7(1)	0.014(1)	^{73}Ge(n, γ)^{74}Ge	1204.2	
		^{200}Tl(EC)^{200}Hg	1205.70(9)	
1221.45(4)	0.039(1)	^{182}Ta(β^-)^{182}W	1221.4066(17)	
1231.0(2)	0.011(1)	^{182}Ta(β^-)^{182}W	1231.0156(17)	
1238.4(1)	0.015(1)	^{214}Bi(β^-)^{214}Po	1238.11(1)	^{238}U series
		^{56}Co(EC)^{56}Fe	1238.282(7)	weak
		^{201}Pb(EC)^{201}Tl	1238.76(7)	weak
1274.05(9)	0.027(1)	?	?	blend
		^{22}Na(EC)^{22}Ne	1274.53(2)	blend
1276.8(5)	0.004(1)	^{201}Pb(EC)^{201}Tl	1277.13(7)	blend
1290.8(3)	0.008(1)	?	?	blend
1293.4(1)	0.024(2)	^{41}Ar(β^-)^{41}K	1293.64(4)	blend
1298.63(8)	0.019(1)	?	?	
1312.10(7)	0.022(1)	^{48}V(EC)^{48}Ti	1312.096(6)	
		^{48}Sc(β^-)^{48}Ti	1312.096(6)	
		^{48}V(EC)^{48}Ti + L	1312.6	

Table 1. continued.

Measured		Parent	Nominal	Comment
Energy [keV]	Count rate [cts/sec]	process	energy [keV]	
1316.6(3)	0.005(1)	?	?	
		^{48}V(EC)^{48}Ti + K	1317.062(6)	
1332.5(1)	0.013(1)	^{60}Co(β^-)^{60}Ni	1332.492(4)	
1336.82(2)	0.109(2)	^{69}Ge(EC)^{69}Ga	1347.09(6)	
		^{69}Ge(EC)^{69}Ga + L	1348.3	
		?	?	
1345.4(4)	0.017(8)	?	?	blend
1347.04(6)	0.147(9)	^{69}Ge(EC)^{69}Ga + K	1347.09(6)	blend
1354.2(4)	0.005(1)	?	?	
1357.0(3)	0.006(1)	?	?	
1364.4(2)	0.008(1)	?	?	
1368.650(9)	0.201(2)	^{24}Na(β^-)^{24}Mg	1368.626(5)	
1377.89(6)	0.033(1)	^{214}Bi(β^-)^{214}Po	1377.669(12)	^{238}U series
1381.79(3)	0.064(2)	^{48}Ti(n, γ)^{49}Ti	1381.745(4)	
1394.6(6)	0.003(1)	^{21}F(β^-)^{21}Ne	1395.131(17)	
1397.7(4)	0.005(1)	?	?	
1408.1(3)	0.005(1)	^{214}Bi(β^-)^{214}Po	1407.98(4)	^{238}U series
1434.15(2)	0.072(1)	^{52}V(β^-)^{52}Cr	1434.068(14)	PSD
		^{52}Mn(EC)^{52}Cr	1434.068(14)	PSD, weak
1460.80(2)	0.114(2)	^{40}K(EC)^{40}Ar	1460.822(6)	PSD, natural radioactivity
1481.1(3)	0.005(1)	?	?	PSD
1497.7(3)	0.005(1)	?	?	PSD, blend
1501.5(2)	0.006(1)	?	?	PSD, blend
1525.5(1)	0.0132(9)	^{69}Ge(EC)^{69}Ga	1525.83(7)	PSD
		^{69}Ge(EC)^{69}Ga + L	1527.0	PSD
1536.33(4)	0.035(1)	^{69}Ge(EC)^{69}Ga + K	1536.20(7)	PSD
		^{203}Bi(EC)^{203}Pb	1536.4(4)	PSD
1552.1(2)	0.012(1)	?	?	PSD
1580.4(3)	0.007(1)	?	?	PSD, blend
1587.5(1)	0.024(1)	?	?	PSD, blend
1609.1(2)	0.018(1)	?	?	PSD, blend
1613.1(1)	0.029(2)	^{56}Fe(n, γ)^{57}Fe	1612.8	PSD, blend
1620.7(2)	0.009(1)	^{212}Bi(β^-)^{212}Po	1620.5(1)	PSD
1630.9(2)	0.013(1)	?	?	PSD, blend
1633.66(3)	0.123(3)	^{20}Ne*	1633.602(15)	PSD, blend
		^{20}F(β^-)^{20}Ne	1633.602(15)	PSD
1648.3(4)	0.004(1)	?	?	
1658.4(1)	0.014(1)	?	?	
~1670–1700		^{58}Co(EC)^{58}Fe	1674.730(10)	complex
		^{58}Co(EC)^{58}Fe + L	1675.5	complex
		^{58}Co(EC)^{58}Fe + K	1681.843(10)	complex
1719.0(2)	0.005(1)	^{206}Bi(EC)^{206}Pb	1718.70(7)	
		^{203}Bi(EC)^{203}Pb	1719.7(4)	
1724.9(2)	0.005(1)	^{56}Fe(n, γ)^{57}Fe	1725.09(6)	
1729.5(1)	0.0087(7)	?	?	
1758.3(3)	0.005(1)	?	?	
1764.34(2)	0.222(4)	^{205}Bi(EC)^{205}Pb	1764.36(4)	
		^{214}Bi(β^-)^{214}Po	1764.494(14)	^{238}U series
1776.00(7)	0.039(2)	^{205}Bi(EC)^{205}Pb	1775.79(4)	blend
1778.961(8)	0.365(4)	^{28}Al(β^-)^{28}Si	1778.969(12)	blend
1805.8(3)	0.007(1)	?	?	blend
1808.7(1)	0.029(2)	^{26}Na(β^-)^{26}Mg	1808.66(3)	blend
		^{26}Mg*	1808.66(3)	blend
1810.9(2)	0.017(2)	^{56}Mn(β^-)^{56}Fe	1810.772(17)	blend
1832.3(1)	0.007(1)	?	?	
1847.4(2)	0.0072(7)	^{203}Bi(EC)^{203}Pb	1847.4(3)	
		^{214}Bi(β^-)^{214}Po	1847.42(3)	^{238}U series
1861.7(2)	0.005(1)	?	?	

Table 1. continued.

Measured		Parent	Nominal	Comment
Energy [keV]	Count rate [cts/sec]	process	energy [keV]	
1882.5(2)	0.007(1)	^{66}Ga(EC)^{66}Zn + K	1882.440(3)	sum peak
		?	?	
1888.0(2)	0.0087(7)	^{203}Bi(EC)^{203}Pb	1888.2(3)	blend
1892.37(9)	0.0176(8)	^{69}Ge(EC)^{69}Ga	1891.55(7)	blend
		^{69}Ge(EC)^{69}Ga + L	1892.8	blend
		^{203}Bi(EC)^{203}Pb	1893.0(3)	blend
1901.85(9)	0.0170(9)	^{69}Ge(EC)^{69}Ga + K	1901.92(7)	
1919.8(3)	0.005(1)	?	?	
1923.8(4)	0.0051(8)	^{69}Ge(EC)^{69}Ga	1923.8(2)	
		^{69}Ge(EC)^{69}Ga + L	1925.0	
1927.5(4)	0.004(1)	?	?	
1934.13(9)	0.0140(8)	^{69}Ge(EC)^{69}Ga + K	1934.2(2)	
1940.9(3)	0.004(1)	?	?	
1964.9(2)	0.005(1)	?	?	
2011.6(6)	0.0023(8)	?	?	
		^{203}Bi(EC)^{203}Pb	2011.4(6)	
2024.00(1)	0.013(1)	^{69}Ge(EC)^{69}Ga	2023.99(13)	
		^{69}Ge(EC)^{69}Ga + L	2025.2	
2033.95(9)	0.017(1)	^{69}Ge(EC)^{69}Ga + K	2034.36(13)	
2113.0(2)	0.0068(7)	^{56}Mn(β^-)^{56}Fe	2113.123(10)	
2117.7(5)	0.0022(6)	?	?	
2167.3(3)	0.0039(7)	?	?	
~2195–2223		^{214}Bi(β^-)^{214}Po	2204.21(4)	complex, ^{238}U series
		^{27}Al*	2211.0(7)	complex, kinematically broadened
2223.42(2)	0.1086(9)	^{1}H(n, γ)^{2}D	2223.255(4)	complex
2236.8(2)	0.0052(6)	?	?	
2295.5(4)	0.0035(6)	^{48}V(EC)^{48}Ti	2295.625(7)	blend, sum peak
		^{48}V(EC)^{48}Ti + L	2296.1	blend, sum peak
2300.7(1)	0.0112(7)	^{48}V(EC)^{48}Ti + K	2300.591(4)	blend, sum peak
2319.1(1)	0.0153(7)	?	?	
2390.6(2)	0.0052(5)	?	?	
2448.0(3)	0.0036(5)	?	?	
2507.1(3)	0.0042(5)	?	?	
2512.8(4)	0.0031(5)	?	?	
2528.5(4)	0.0027(5)	?	?	
2599.5(3)	0.0039(5)	?	?	
2614.61(3)	0.0380(6)	^{208}Tl(β^-)^{208}Pb	2614.533(13)	natural radioactivity
2657.3(3)	0.0031(5)	^{56}Mn(β^-)^{56}Fe	2657.45(5)	
2741.7(3)	0.0037(4)	?	?	
2749.9(2)	0.0120(9)	?	?	blend
		^{66}Ga(EC)^{66}Zn	2751.852(6)	blend
		^{66}Ga(EC)^{66}Zn + L	2753.0	blend
2754.03(1)	0.153(1)	^{24}Na(β^-)^{24}Mg	2754.01(1)	blend
2761.4(1)	0.0082(4)	^{66}Ga(EC)^{66}Zn + K	2761.511(6)	
2959.5(5)	0.0048(6)	?	?	
2982.0(7)	0.0028(5)	?	?	
~2993–3013		^{27}Al*	3004.3	complex, kinematically broadened
3034.2(6)	0.0032(5)	?	?	
3120.0(3)	0.0018(4)	?	?	
3229.1(2)	0.0040(3)	^{66}Ga(EC)^{66}Zn	3228.824(9)	
		^{66}Ga(EC)^{66}Zn + L	3229.9	
		^{48}V(EC)^{48}Ti + K	3228.858(11)	
3238.2(1)	0.0066(4)	^{66}Ga(EC)^{66}Zn + K	3238.483(6)	
3381.2(2)	0.0046(4)	^{66}Ga(EC)^{66}Zn	3380.88(1)	
		^{66}Ga(EC)^{66}Zn + L	3381.2	
3390.2(2)	0.0037(3)	^{66}Ga(EC)^{66}Zn + K	3390.54(1)	
3451.7(5)	0.0013(3)	^{56}Co(EC)^{56}Fe	3451.152(17)	
		^{56}Co(EC)^{56}Fe + K	3452.42(1)	sum peak

Table 1. continued.

Measured		Parent	Nominal	Comment
Energy [keV]	Count rate [cts/sec]	process	energy [keV]	
3791.4(1)	0.0085(3)	^{66}Ga(EC)^{66}Zn	3791.036(8)	
		^{66}Ga(EC)^{66}Zn + L	3792.1	
3800.26(4)	0.0220(4)	^{66}Ga(EC)^{66}Zn+ K	3800.695(8)	
3852.4(5)	0.0015(3)	^{13}C*	3853.170(22)	
4085.8(2)	0.0045(3)	^{66}Ga(EC)^{66}Zn	4085.875(12)	
		^{66}Ga(EC)^{66}Zn + L	4087.0	
4095.4(2)	0.0048(3)	^{66}Ga(EC)^{66}Zn + K	4095.543(12)	
4122.14(7)	0.0105(3)	^{24}Na(β^-)^{24}Mg	4122.633(12)	sum peak
4295.27(7)	0.0137(4)	^{66}Ga(EC)^{66}Zn	4295.224(10)	
		^{66}Ga(EC)^{66}Zn + L	4296.3	
4304.54(6)	0.0151(3)	^{66}Ga(EC)^{66}Zn + K	4304.883(10)	
4434.(3.)	0.021(2)	^{12}C*	4438.03(31)	kinematically broadened, FWHM ~90 keV
4461.1(2)	0.0035(3)	^{66}Ga(EC)^{66}Zn	4461.247(13)	
		^{66}Ga(EC)^{66}Zn + L	4462.3	
4470.6(2)	0.0030(2)	^{66}Ga(EC)^{66}Zn + K	4470.906(13)	
4805.9(1)	0.0057(3)	^{66}Ga(EC)^{66}Zn	4806.060(18)	
		^{66}Ga(EC)^{66}Zn + L	4807.2	
4815.2(1)	0.0061(3)	^{66}Ga(EC)^{66}Zn + K	4815.719(18)	
4881.9(4)	0.0009(2)	?	?	
5269.1(3)	0.0017(2)	^{15}N*	5269.161(14)	
5297.7(4)	0.0016(2)	^{15}C(β^-)^{15}N	5297.817(14)	
5450.7(4)	0.0013(2)	?	?	
5518.0(4)	0.0024(3)	^{72}Ge(n, γ)^{73}Ge	5518.3	
5529.(1.)	0.0010(2)	?	?	
5618.1(2)	0.0037(3)	^{52}Cr(n, γ)^{53}Cr	5618.2	
		^{16}O*	~5617.6	single escape
		^{16}N(β^-)^{16}O	~5617.6	single escape
5910.8(2)	0.0056(3)	?	?	
5920.2(4)	0.0021(2)	^{56}Fe(n, γ)^{57}Fe	5920.45(2)	
5994.6(4)	0.0014(2)	^{74}Ge(n, γ)^{75}Ge	~5994.1	single escape
6018.9(5)	0.0011(2)	^{56}Fe(n, γ)^{57}Fe	6018.4	
6036.7(6)	0.0009(2)	?	?	
~6105–6129		^{70}Ge(n, γ)^{71}Ge	6116.9	complex
6128.94(4)	0.0283(4)	^{16}O*	6128.63(4)	
		^{16}N(β^-)^{16}O	6128.63(4)	
6204.5(4)	0.0018(2)	?	?	
		^{72}Ge(n, γ)^{73}Ge	~6206.0	single escape
6250.7(2)	0.0043(2)	?	?	
		^{48}Ti(n, γ)^{49}Ti	~6249.1	single escape
6276.1(7)	0.0012(2)	?	?	
6320.2(5)	0.0015(2)	?	?	
6365.1(3)	0.0025(2)	^{74}Ge(n, γ)^{75m}Ge	6365.4	S_n − 139.69 keV
6391.7(4)	0.0018(2)	?	?	
		^{72}Ge(n, γ)^{73}Ge	6390.2	
		^{70}Ge(n, γ)^{71}Ge	~6393.6	double escape
6418.0(1)	0.0063(3)	^{72}Ge(n, γ)^{73}Ge	6418.6	
		^{48}Ti(n, γ)^{49}Ti	6418.4	
6499.6(6)	0.0023(4)	?	?	blend
6505.3(1)	0.0153(4)	^{74}Ge(n, γ)^{75}Ge	6505.1	blend, S_n
6556.2(5)	0.0015(2)	^{48}Ti(n, γ)^{49}Ti	6555.9	
6707.7(3)	0.0037(3)	^{70}Ge(n, γ)^{71}Ge	6707.5	blend
6716.1(1)	0.0155(5)	?	?	blend
		^{72}Ge(n, γ)^{73}Ge	6717.0	blend
6753.9(5)	0.0023(3)	?	?	blend
6760.3(1)	0.0164(4)	^{48}Ti(n, γ)^{49}Ti	6760.1	blend
6770.9(6)	0.0012(2)	?	?	blend
6781.5(3)	0.0025(2)	?	?	blend
6809.8(1)	0.0049(2)	^{9}Be(n, γ)^{10}Be	6809.9	S_n

Table 1. continued.

Measured		Parent	Nominal	Comment
Energy [keV]	Count rate [cts/sec]	process	energy [keV]	
6837.7(3)	0.0025(2)	^{62}Ni(n, γ)^{63}Ni	6837.4	
6904.5(3)	0.0035(2)	^{70}Ge(n, γ)^{71}Ge	~6904.6	single escape
6915.6(5)	0.0014(2)	^{70}Ge(n, γ)^{71}Ge	6915.7	
7119.5(2)	0.0063(3)	^{56}Fe(n, γ)^{57}Fe	~7120.2	single escape
7134.3(3)	0.0041(2)	^{56}Fe(n, γ)^{57}Fe	~7134.6	single escape
7159.9(9)	0.0012(2)	?	?	
7214.5(3)	0.0036(3)	^{27}Al(n, γ)^{28}Al	~7212.9	single escape
		^{70}Ge(n, γ)^{71}Ge	7217.2	S_n − 198.4 keV
7243.4(4)	0.0026(3)	^{55}Mn(n, γ)^{56}Mn	7243.4	
7276.7(6)	0.0018(2)	?	?	
		^{56}Fe(n, γ)^{57}Fe	7278.8	
7306.8(8)	0.0013(2)	^{63}Cu(n, γ)^{64}Cu	7307.3	
~7400-7415		^{63}Cu(n, γ)^{64}Cu	~7405.3	complex, single escape
7415.66(6)	0.0307(5)	^{70}Ge(n, γ)^{71}Ge	7415.6	complex, S_n cascade
7426.9(5)	0.0014(2)	^{52}Cr(n, γ)^{53}Cr	~7427.6	single escape
7623.3(4)	0.0031(3)	?	?	blend
7631.5(1)	0.0228(4)	^{56}Fe(n, γ)^{57}Fe	7631.2	blend
7645.7(1)	0.0188(4)	^{56}Fe(n, γ)^{57}Fe	7645.6	S_n
7694.1(5)	0.0013(2)	^{27}Al(n, γ)^{28}Al	7693.4	
7716.0(9)	0.0011(2)	?	?	blend
7724.4(1)	0.0112(3)	^{27}Al(n, γ)^{28}Al	7724.0	blend, S_n
7819.0(4)	0.0014(2)	^{60}Ni(n, γ)^{61}Ni	7819.4	
7910.5(4)	0.0025(3)	?	?	blend
7915.7(1)	0.0100(3)	^{63}Cu(n, γ)^{64}Cu	7916.3	blend, S_n
7939.3(3)	0.0023(2)	^{52}Cr(n, γ)^{53}Cr	7938.6	
8488.(1.)	0.0011(2)	^{58}Ni(n, γ)^{59}Ni	~8487.4	multiple, single escape
8578.(1.)	0.0011(2)	?	?	multiple
8998.0(4)	0.0027(3)	^{58}Ni(n, γ)^{59}Ni	8998.4	multiple, S_n
9598.3(9)	0.0006(1)	^{73}Ge(n, γ)^{74}Ge	9600.2	multiple, S_n − 595.8 keV
9683.6(9)	0.0006(1)	^{73}Ge(n, γ)^{74}Ge	~9685.2	multiple, single escape
10195.0(4)	0.0057(3)	^{73}Ge(n, γ)^{74}Ge	10196.2	multiple, S_n

The meaning of standardized comments in Col. 5 is as follows:
– *blend*: a line-like feature consisting of a few components that blend because they are closely spaced in energy; resolving the components can be very difficult and systematic uncertainties can be much larger than the quoted statistical errors.
– *complex*: a complex spectral feature which can result from the blending of many lines, from the presence of a single broad structure, or both; sometimes the complex is named for its dominant component.
– *weak*: indicates a contribution to a line that is expected to be significantly weaker than all other contributions.
– *sum peak*: the peak results from the coincident interaction of two gamma rays from the same de-excitation cascade.
– *natural radioactivity*: the parent isotope is so-called “naturally” radioactive, i.e. it is not radioactive because of activation processes in orbit.
– *. . . series*: similar to above, except that the parent isotope is a member of the quoted so-called natural decay series.
– *saw tooth*: a saw tooth or triangular shaped spectral feature due to inelastic neutron scattering in the Ge detector, the saw tooth results from the summation of the gamma-ray energy and the recoil energy of the excited Ge nucleus.
– *PSD*: the line rate has been corrected for the efficiency of the PSD electronics.
– *single/double escape*: single/double escape peak.
– *multiple*: the line occurs only in multiple event data, the quoted rate is for the sum of double and triple events.
– S_n: when a thermal neutron is captured, the excitation energy of the product nucleus is equal to its neutron separation energy S_n; in the table S_n denotes lines which arise from de-excitations via a single (or a few) transition(s) after thermal neutron capture.